









RESEARCH ARTICLE | NOVEMBER 14 2024

Development of a compact and portable diamond-based detection system for dosimetry and microdosimetry in ion beam therapy

C. Verona ; A. Fabbri ; A. Fazzi ; L. Bianchi ; V. Conte ; G. Petringa ; A. Raso ; G. Verona Rinati 



Rev. Sci. Instrum. 95, 113302 (2024)

<https://doi.org/10.1063/5.0235400>



Articles You May Be Interested In

A diamond guard ring microdosimeter for ion beam therapy

Rev. Sci. Instrum. (May 2020)

Spectroscopic properties and radiation damage investigation of a diamond based Schottky diode for ion-beam therapy microdosimetry

J. Appl. Phys. (November 2015)

A 3D lateral electrode structure for diamond based microdosimetry

Appl. Phys. Lett. (January 2017)



Special Topics Open for Submissions

[Learn More](#)

Development of a compact and portable diamond-based detection system for dosimetry and microdosimetry in ion beam therapy

Cite as: *Rev. Sci. Instrum.* **95**, 113302 (2024); doi: [10.1063/5.0235400](https://doi.org/10.1063/5.0235400)

Submitted: 27 August 2024 • Accepted: 20 October 2024 •

Published Online: 14 November 2024



View Online



Export Citation



CrossMark

C. Verona,^{1,a)} A. Fabbri,² A. Fazzi,³ L. Bianchi,² V. Conte,⁴ G. Petringa,⁵ A. Raso,¹
and G. Verona Rinati¹

AFFILIATIONS

¹Dipartimento di Ingegneria Industriale, Università di Roma "Tor Vergata," Sez. INFN-Roma2, 00133 Rome, Italy

²INFN Roma Tre, 00146 Rome, Italy

³Politecnico di Milano, Dipartimento di Energia, via Lambruschini 4, INFN-Sezione di Milano, 20156 Milano, Italy

⁴INFN Laboratori Nazionali di Legnaro, viale dell'Università 2, 35020 Legnaro (PD), Italy

⁵INFN Laboratori Nazionali del Sud, via S. Sofia 62, 95123 Catania, Italy

^{a)} Author to whom correspondence should be addressed: claudio.verona@uniroma2.it

ABSTRACT

Ion beam therapy techniques have advanced significantly in the past two decades. However, the development of dosimetric verification methods has lagged. Traditional dosimetry, which offers a macroscopic view of the absorbed dose, fails to address the micrometric-scale stochastic effects crucial for understanding biological responses. To bridge this gap, microdosimeters are used to assess physical quantities correlated with radiation effects. This work reports on the design and testing of a novel detection system based on synthetic single crystal diamond. The system is capable of simultaneously performing dosimetric and microdosimetric characterizations of clinical ion beams. The detector incorporates two active components configured as diamond Schottky diodes, both integrated on a single crystal diamond substrate. In particular, one very small element (sensitive area 0.0078mm^2) was designed to evaluate microdosimetric metrics, while the other large one (sensitive area 4.2mm^2) was designed to measure the absorbed dose to water. Diamond detectors were characterized using the ion beam induced charge (IBIC) technique, employing a 1 MeV protons microbeam. The IBIC map of the diamond detector shows two distinct sensitive areas with quite uniform sensitivity, well contained within the metallic contact regions. Dedicated front-end electronic circuits were designed and implemented for both the dosimetric and microdosimetric signals. These circuits, along with the integrated diamond detector, were embedded in an aluminum waterproof housing to minimize electronic interference. This configuration enables a compact, portable setup compatible with water phantoms. Laboratory tests with alpha particles yielded promising results, demonstrating stable and reproducible responses with a good signal-to-noise ratio.

© 2024 Author(s). All article content, except where otherwise noted, is licensed under a Creative Commons Attribution (CC BY) license (<https://creativecommons.org/licenses/by/4.0/>). <https://doi.org/10.1063/5.0235400>

I. INTRODUCTION

The use of proton and ion beams for cancer treatment has significantly increased in recent years, as evidenced by the growing number of particle therapy centers worldwide. In Europe alone, 24 particle therapy facilities were built between 2009 and 2023.¹ Proton and ion beam therapies offer significant advantages over

conventional photon radiation therapy, primarily due to the unique depth-dose characteristics of these particles. Unlike photon beams, whose depth-dose profile gradually decreases as they penetrate deeper, that of particle beams increases with depth and sharply drops at a given depth, allowing for precise targeting of tumors and minimizing damage to adjacent healthy tissues.^{2,3} However, these therapies are not without risks, including potential necrosis

of healthy tissue near the treatment area and the risk of inducing secondary cancers, influenced by the radiation dose, volume, and region irradiated.^{4,5}

The absorbed dose, measured by commercial dosimeters, such as ionization chambers or solid-state dosimeters, serves as the primary measure for clinical prescriptions, correlating well with biological damage in conventional photon and electron therapies. For particle therapies, instead, the absorbed dose alone does not sufficiently describe the biological effects. High linear energy transfer (LET) particles cause concentrated energy deposition along their trajectories, resulting in more severe damage than low LET particles for the same absorbed dose. This difference in biological effectiveness is expressed as the particle's relative biological effectiveness (RBE), a crucial parameter defined as the ratio of the doses (that of the particle under examination and that of the reference radiation) required to produce the same level of biological damage. RBE compares the effects of high LET radiation to reference photon radiation and depends on several factors, such as tissue type and beam quality.^{6,7} Treatment planning procedures in ion beam therapy are based on the product of the absorbed dose and appropriate weighting factors that account for the RBE of the radiation. These factors are derived from radiobiological data obtained by irradiating thin biological samples with diverse types of radiation of known LET. Alternatively, microdosimetry was developed to supplement traditional dosimetry by providing physical quantities linked to RBE. A single semiconductor detector (i.e., MOS-FET) capable of performing both dosimetry and microdosimetry simultaneously at the same position were introduced by Rosenfield *et al.*,⁸ offering an efficient method for mixed radiation fields in therapeutic context.

Microdosimeters measure the probability distribution of imparted energy within a microscopic sensitive volume (SV), offering insights into the stochastic aspects of radiation interaction. The development of microdosimeters that can be directly used in therapeutic beams is becoming increasingly relevant today, extending beyond the characterization of RBE.^{9,10} While Tissue Equivalent Proportional Counters (TEPCs) are well-established microdosimeters, solid-state microdosimeters are increasingly used due to their higher spatial resolution, low-voltage operation, transportability, cost-effectiveness, and ease-of-use.^{11,12}

Among the solid-state detectors, single-crystal synthetic diamond detectors represent a promising solution for both dosimetry and microdosimetry. Diamond, with its unique physical properties, such as high radiation hardness and near tissue equivalence, offers significant advantages over traditional silicon detectors, which require corrections for non-tissue equivalence and exhibit lower radiation hardness. Its radiation hardness ensures long-term stability and reliability under high-radiation conditions without significant degradation, making it ideal for use in ion therapy beams.¹³ Its near tissue equivalence (similar atomic number to human tissue) and nearly constant ratio between stopping power with water for particles provide accurate dosimetric and microdosimetric measurements.¹⁴ Diamond's low dielectric constant and high bandgap result in minimal noise and high signal integrity, crucial for precise dosimetric readings. While diamond dosimeters, and in particular the microDiamond detector (model 60019, PTW Freiburg), developed by the University of Rome Tor Vergata in collaboration with PTW-Freiburg, is widely diffused and well-established

in clinical practice worldwide,^{15,16} diamond microdosimeters have been recently proposed for particle therapy applications in various configurations.¹⁷⁻¹⁹ The microdosimetric properties of diamond, along with its excellent dosimetric performance, enhance the potential for diamond detectors that can perform both dosimetric and microdosimetric characterizations of radiation beams as recently reported in the literature.^{20,21}

In this work, we report the development and preliminary test of a novel detection system based on synthetic single crystal diamond, capable of simultaneously performing dosimetric and microdosimetric characterizations of clinical ion beams. The work included the fabrication and characterization of diamond detectors and the design of dedicated and optimized electronic readout chains, placed close to the diamond detectors to minimize pickup noise and ensure accurate data collection. The integration between diamond and front-end electronics is housed in a waterproof casing, resulting in a compact, user-friendly, and portable detection system capable of accurate measurements in clinical settings. In addition, the use of a single embedded device that operates simultaneously in both modalities allows for shortening measurement time and reducing experimental uncertainties, particularly those related to detector positioning. This is crucial in microdosimetry, where energy spectra are often acquired in high LET gradient regions, such as at the end of the Bragg peak curve, making accuracy of primary importance to ensure a correct RBE assessment.

II. MATERIALS AND METHODS

A. Diamond integrated detectors

The diamond detectors were fabricated as a monolithic structure utilizing microwave-enhanced chemical vapor deposition (CVD) of synthetic single crystal diamonds in combination with photolithography techniques at the laboratories of the Industrial Engineering Department of Rome Tor Vergata University. This integrated approach resulted in two active and individual elements, specifically designed as Schottky diodes in a boron-doped/intrinsic diamond/Cr configuration, being embedded on a $3 \times 3 \times 0.3 \text{ mm}^3$ commercial low-cost single-crystal diamond substrate. The two detectors were designed with varying SV and shapes tailored to their specific applications. The fabrication process consists of CVD growth of both boron-doped and high-quality intrinsic diamond by using 200 nm of chromium layers as plasma-resistant masks, facilitating the selective deposition of synthetic diamonds. The boron-doped diamond layer, which acts as a back contact, is $\sim 0.4 \mu\text{m}$ in thickness. The intrinsic diamond layer, which acts as a sensitive layer, has a thickness in the range 1–10 μm . For further details of the technological process, please refer to Ref. 20.

The sketch of the dosimeter and microdosimeter detector is shown in Fig. 1(a).

Each diamond sample consists of two independent detectors.

- (a) A large detector features a donut-shaped contact with an SV of $\sim 4.2 \text{ mm}^2$ cross sectional area (A_{Dos}) and a thickness of $1.0 \pm 0.2 \mu\text{m}$, intended for dosimetric measurements (hereinafter called Dos).
- (b) A small detector with a circular-shaped diamond micro-SV with 100 μm diameter (0.00785 mm^2 cross sectional area)

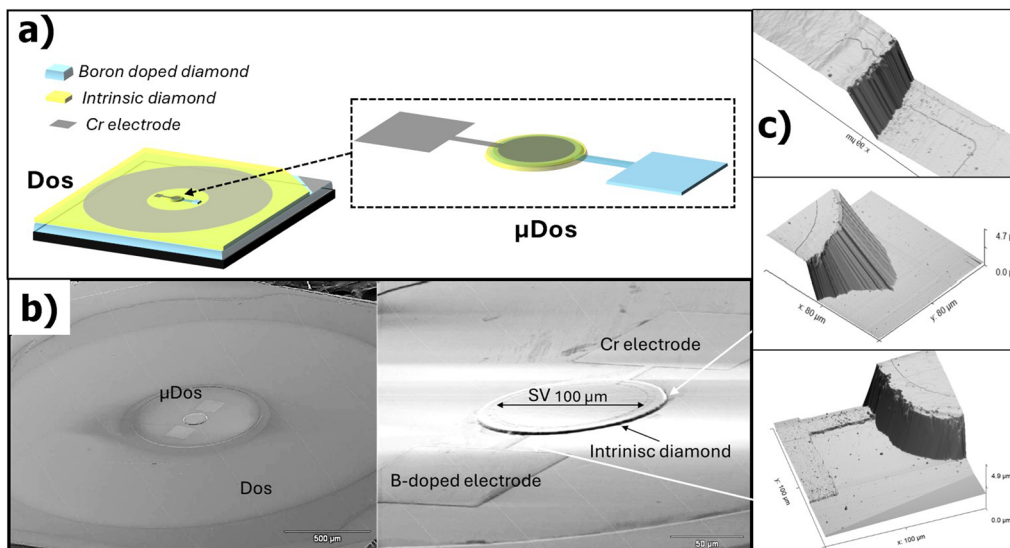


FIG. 1. (a) Sketch and (b) SEM picture of the Dos- μ Dos detector. (c) AFM maps of the SV of the μ Dos device.

and thicknesses in the range of 2–10 μm , designed for microdosimetric measurements (hereinafter called μ Dos). Relatively small thicknesses, i.e., 2–4 μm , are used for high LET particles, such as carbon or oxygen ions, while larger thicknesses can be used for low LET particles, such as protons and helium ions.

A scanning electron microscope (SEM) image of the entire Dos- μ Dos device, along with an enlarged view of the μ Dos positioned at the center of the substrate, is shown in Fig. 1(b). Figure 1(c) shows atomic force microscope (AFM) images of the SV of the μ Dos, which were used to measure the thickness of the deposited layers. Owing to the built-in potential of around 1.3 V at the Cr/intrinsic diamond interface,²² the detector operates as a Schottky diode and can work without the need for an external bias voltage.

In the experiments, the Dos, notable for its very thin diamond layer, is used without bias, while an electric field of 3 V/ μm is applied to the μ Dos to extend the depletion region throughout its entire thickness and to achieve 100% charge collection efficiency (CCE).

B. Electronic read-out systems

The electronic readout circuit for the dosimeter (or Dos) detector was developed to precisely measure the charge generated by the diamond device, which is proportional to the absorbed dose. Figure 2 shows a representation of the Dos front-end and block schematics of the whole Dos electronic chain. The current range varies from few tens of fA, i.e., the diamond dark current, to tens of nA near the Bragg peak of high LET particles. To ensure the appropriate precision over six orders of magnitude of the input signal, a charge integrator scheme was used as the Dos front-end. The use of a small feedback capacitance (100 pF) gives the charge

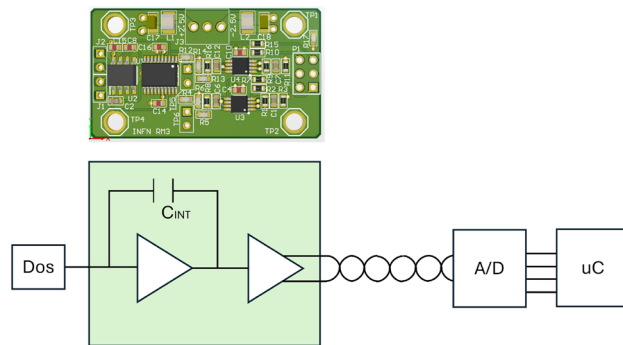


FIG. 2. Representation of the Dos front-end board (top) and a sketch of the Dos whole acquisition chain (bottom).

integrator the needed sensitivity, which can be further enhanced by increasing the integration time, ranged between 100–500 ms. A shorter integration time can be used to avoid the integrator saturation.

An external micro-controller (8.5 × 3.5 × 6.5 cm³ in size) manages the integration time other than a 16-bit A/D converter that acquires the integrator output values both at the start and at the end of each integration period, which is delimited by two reset pulses. The two samplings are made 200 μs after the first reset and 200 μs before the second one, implementing the correlated double sampling (CDS) technique. A dedicated MOS-based circuit allows a fast reset of the capacitor (<1 μs) making the dead-time of the system negligible. Moreover, a single-ended to differential output operational amplifier (usually called ADC driver) stage is present if the charge integrator output signal has to be driven to a remote A/D converter several meters away. This scenario can be quite common when a

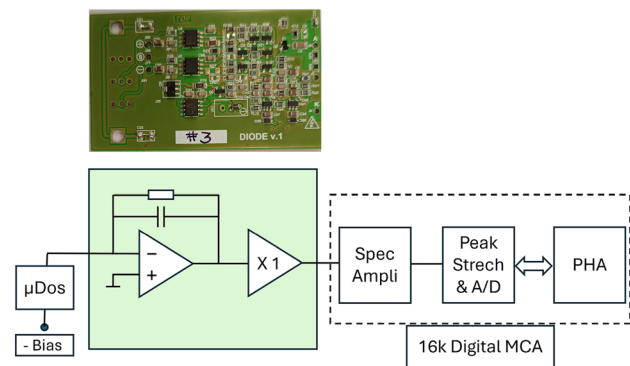


FIG. 3. Picture of the CSP (top) and a sketch of the μ Dos electronic acquisition chain (bottom).

water phantom is used. Data acquisition and settings were managed by custom-developed software. The μ Dos electronic chain consists of a charge sensitive preamplifier (CSP), followed by a spectroscopy amplifier and pulse height analyzer. The front-end electronics is a custom CSP board integrated in the same housing of the detector board, minimizing the capacitance of the electrical connections. The rest of the chain can be realized with commercial standard modules or with a compact digital multi-channel analyzer (MCA) (e.g., Caen DT5770, $10 \times 4 \times 13 \text{ cm}^3$ in size).

The custom CSP must fulfill the main requirements of this specific application: very good linearity, large dynamic range (for decades), and very low noise. The choice of the value of the feedback capacitance and, therefore, of the sensitivity, is crucial for the dynamic and the noise performance trade-off. A high sensitivity of about 7.7 V/pC has been chosen. The discrete technology has been preferred to the integrated one in the design and production of the CSP for many reasons: faster development cycle, less expensive prototyping, single channel electronics, and higher voltage power supply for larger dynamic range. Figure 3 shows the sketch and a photo of the developed CSP.

The input device of the amplifying block is the BF 862 N-channel JFET. The feedback, in addition to the capacitance, comprises a $1 \text{ G } \Omega$ SMT resistor. An output buffer drives the potentially long output coaxial cable. The board dual power supply is at 12 V ; it is internally regulated to dual 11 V allowing maximum output signal amplitude of about 10 V . The noise has been extensively characterized both under open circuit conditions and when connected to the detector board. The measured equivalent noise charge (ENC) is ~ 100 and $140 \text{ RMS electrons}$, respectively, at a $1 \mu\text{s}$ shaping time. This noise level gives an energy resolution of about 4.3 keV_{FWHM} in diamonds. An external test input is available for functional tests and calibration verification.

C. Integration

The Dos- μ Dos detector was wire-bonded onto a printed circuit board made of Teflon, which was then framed with a polymethyl methacrylate (PMMA) border measuring $2.5 \times 2.5 \text{ cm}^2$ and with a thickness of 2.5 mm . This PMMA frame can be filled with epoxy resin, ensuring that $\sim 2.6 \text{ mm}$ of water equivalent layer covered the diamond surface to avoid the effects of air ionization on

the dosimetric response and to ensure the detector is waterproof. The entire assembly, along with the dedicated front-end electronics, was then placed in a specifically designed aluminum housing ($65 \times 160 \times 20 \text{ mm}^3$ in size) realized using a computer numerical control machine. The design includes a 1.5 cm diameter opening, where the detector is located, reducing ion interactions with aluminum and minimizing the contribution of secondary events in the detector's SV. The housing is equipped with O-rings to ensure a watertight seal, allowing measurements to be taken in water phantoms typically used in ion beam therapy centers. The case also includes four LEMO connectors: two for the output signals from the Dos and μ Dos electronic board, one for the polarization of the μ Dos, and one for the reset signal for the Dos charge integrator. In addition, a six-pin connector was used to power the electronic boards with $\pm 12 \text{ V}$ and $\pm 6 \text{ V}$ relative to a common ground. In Fig. 4, the prototype, referred to as DIODE (*Diamond Integrated device fOr HaDronThErapy*), is shown with all these features. The figure illustrates the detailed construction and connection layout, highlighting the Teflon PCB, the developed front-end electronics, and the various connectors. This comprehensive design ensures the device's robustness and compactness. However, by positioning the electronics close to the detector, it introduces limitations when exposed to larger irradiation fields ($>3 \times 3 \text{ cm}^2$), potentially leading to radiation damage and secondary events from ion interactions with the electronic components. Such an effect could be mitigated using radiation-resistant electronic components and appropriate shielding.

D. Monte Carlo simulation

Monte Carlo simulations were carried out using a Geant4 simulation toolkit²³ to reproduce the energy deposited in the μ Dos. The simulated detector has the structure of the μ DOS described in Sec. II A. The diamond was modeled as carbon with a density of 3.51 g/cm^3 and ionizing potential of 81 eV . The energy deposited was scored by each event into the detector SV. The detector was placed in vacuum cantered in front of a straight-directed monoenergetic beam. The simulations were set with the following Physics Lists.

- G4EmLivermorePhysics for electromagnetic interactions,
- G4HadronElasticPhysicsHP for hadronic elastic interactions, and
- G4HadronPhysicsQGSP_BIC_HP and G4IonBinaryCascadePhysics for hadronic inelastic interactions.

To optimize computational times, production cuts were applied to secondary electron production. In Geant4, a production cut is defined by a length: if a secondary particle's energy corresponds to a range longer than the set cut, it is simulated; otherwise, its energy is considered locally deposited. According to the μ Dos geometry dimensions, the production cut was fixed at $1 \mu\text{m}$ ($\sim 2 \text{ keV}$ energy secondary electron in diamond).

III. RESULTS AND DISCUSSION

The developed Dos- μ Dos detectors were initially characterized at the ion microbeam line of the Laboratori Nazionali di Legnaro

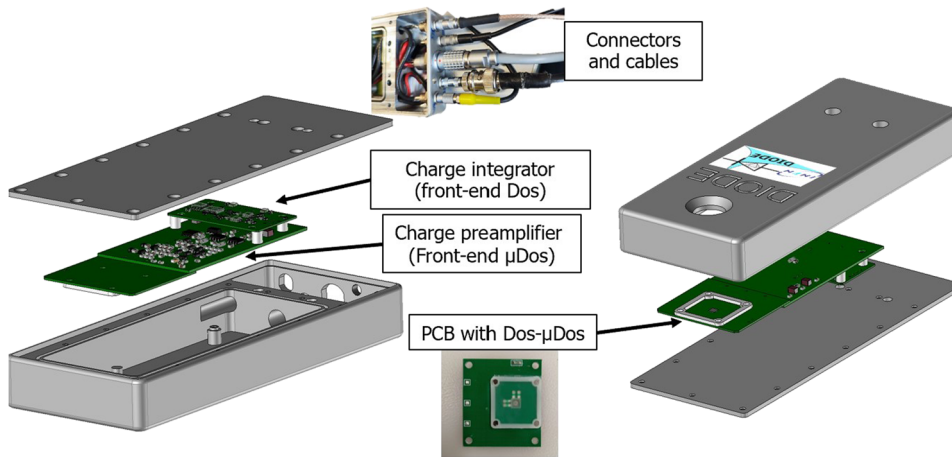


FIG. 4. Schematic representation of the DIODE device as embedded in water-proof Al housing, along with the front-end electronic circuits.

(LNL)-INFN using 1 MeV proton beam with an ions current of 1 nA from a Van de Graaff accelerator (AN2000). The ion beam induced charge (IBIC) characterization was used to assess the detectors' charge collection properties and spatial uniformity, with a resolution linked to the micro-beam spot size ($2\text{--}3\ \mu\text{m}$). This method involves scanning a focused ion beam across the detector surface, precisely positioning it using a magnetic quadrupole lens and a magnetic scanner unit, which are standard components of an ion microprobe facility. For this characterization, the Dos and μDos detectors were connected to two microdosimetric electronic chains and the signals acquired simultaneously. The signals from the two acquisition chains and the beam position (x,y coordinates) were recorded in an event-by-event list mode file. These data were used to create IBIC maps, correlating the spatial energy distribution of the scanned area.²⁴ The energy calibration was performed using a pulse generator and a thick diamond detector with 100% CCE irradiated with the same ion species.

Figure 5 shows a typical large IBIC map ($\sim 3 \times 3\ \text{mm}^3$) of the Dos- μDos detector, featuring sensitive volumes of the two detectors,

oriented as shown in the optical microscope image of Fig. 5. The IBIC map from the Dos- μDos detector demonstrates two distinct and differentiated sensitive areas with a consistently uniform sensitivity, which is well-contained within the metallic contact areas of the two detectors. This indicates that the drift of charge carriers in the depletion region below the Cr electrode generates a clear current signal, while free carriers produced in other areas do not produce detectable signals. In the IBIC map of the Dos, the stripe-shaped regions without events are caused by the Al wires bonding, as can be clearly observed in the optical picture shown in Fig. 5. Indeed, the Al wire, with a thickness of $25\ \mu\text{m}$, is thick enough to entirely stop the protons before they can penetrate the sensitive volume of the detector.

In addition, to better characterize the μDos , an enlarged IBIC map ($400 \times 400\ \mu\text{m}^2$ in size) was also acquired. Figure 6 shows the energy deposition spectra acquired by the diamond μDos with a sensitive thickness of $4.5\ \mu\text{m}$, which exhibit a Gaussian-shaped distribution expected for a mono-energetic beam traversing the detector. In addition, a low-energy tail can be also observed in the

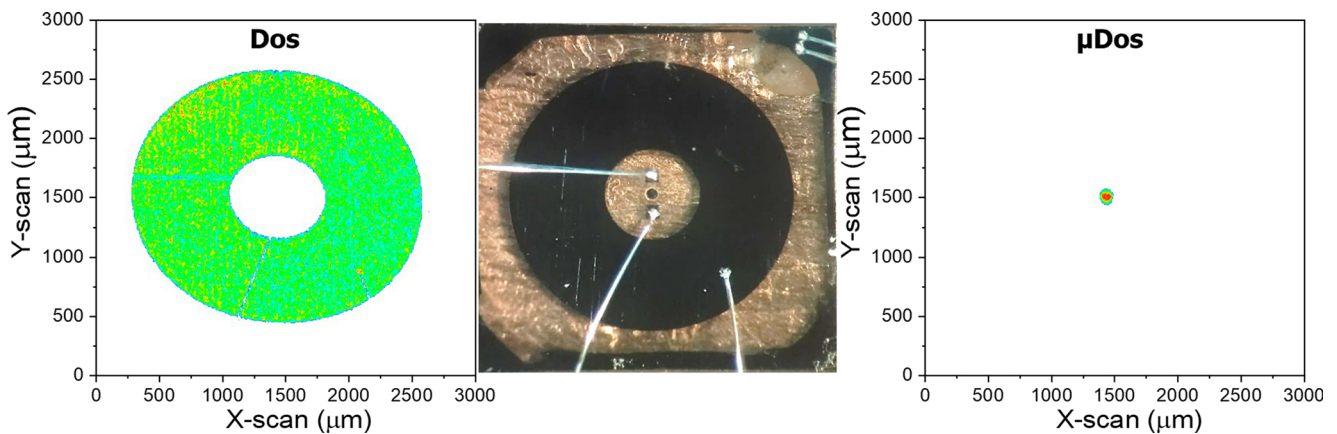


FIG. 5. Large IBIC map of the Dos- μDos device. An optical image of the device is provided as a visual reference.

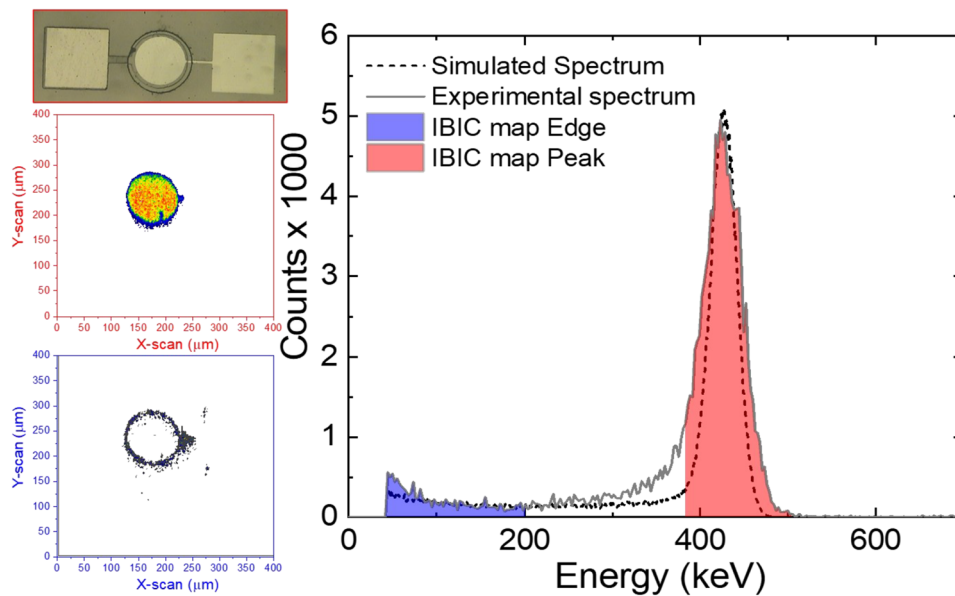


FIG. 6. Energy spectrum recorded by the μ Dos during 1 MeV proton microbeam irradiation, divided into two colored regions. Monte Carlo simulation is also indicated by the dashed line (right). IBIC maps for each region, created from events where energy deposition occurred within the specified region; map contours match the corresponding region color (left).

spectrum. The energy spectrum was divided into two regions, red and blue, to study the origin of the different contributions within the detector. Partial IBIC maps were then created for each region, focusing on events within these energy windows. As clearly shown in Fig. 6, the main peak events (red region) were collected by well-defined SV with a $100\ \mu\text{m}$ diameter, while the blue region indicates incomplete charge collection at the edge of the SV. In addition, a signal is observed in a small region on the right side within the first micrometers from the edge of the SV. This region corresponds to the initial part of the Cr strip connecting the bond pad, which is partially overlapped to the intrinsic diamond layer that is slightly wider than the B-doped diamond electrode size (see the optical image of the microdosimeter shown in Fig. 6).

The energy deposition spectrum of the incident protons was simulated using the Geant4 simulation toolkit, as described in Sec. II D. A good agreement was obtained between the simulated (dotted line) and experimental (continuous line) spectra, indicating that the experimental setup and simulation model are accurately representing the physical processes involved as well as a 100% CCE of the detector. However, the experimental energy distribution shows a marginally larger FWHM compared to the simulated one, primarily ascribed to structural inhomogeneity of the SV's detector and/or electromagnetic noise during the irradiation. After characterizing the integrated diamond detectors, the DIODE prototype was tested in air with 5.47 MeV α -particles irradiation (not collimated) from a ^{241}Am source, placed at 4 mm from the detector surface. By taking into account the absorption of air under the given irradiation conditions, the energy of impinging α -particles was estimated to be 5.1 MeV. The fluence rate ϕ at the detector surface was $\sim 100\ \text{particles}/\text{mm}^2 \cdot \text{s}$. During tests, the output signal waveforms from both detectors were initially acquired by a 200 MHz PicoScope 3000E series, by applying a 3 bit digital filter. Figure 7 shows typical signals from Dos and μ Dos detectors, as processed by the front-end electronics described in Sec. II B. The black line

represents the signal coming from the charge integrator output for a 500 ms integration time. In particular, as described in Sec. II B, it represents the voltage across the 100 pF integrating capacitor. To better separate a single acquisition window, a reset time of 10 ms was adopted for the measurement shown in Fig. 7, instead of the much shorter usual one, i.e., 0.1 ms. It can be seen that although the integration capacitor was chosen with a low hysteresis factor and the reset switch has a very low injected charge, the starting point of the integration cycle is nonzero. However, with the implementation of the double correlated technique, this is not an issue. During the integration interval, an increase in the integrated charge with a nearly constant slope is observed, indicating a nearly constant detector current. Such a signal is generated by a discrete number of impinging α -particles. However, given the relatively large number of α -particles impinging the Dos detector (about 200 in the 500 ms integration time) and the small charge generated by each of them, they are not distinguished, resulting in a continuous increase in the integrated charge. As previously described, the signal is sampled just after the first reset and just before the second one. By considering a difference of about 8 mV between the two samplings over a 100 pF capacitor, the integrated charge is 0.8 pC, corresponding to a detector current of $\sim 1.6\ \text{pA}$.

The blue line shown in Fig. 7 represents the μ Dos output signal, resulting from α -particles impinging on the SV of the μ Dos detector. The output waveform, shown in the inset of Fig. 7, is the typical δ -response of a CSP. The exponential decay time constant of 130 μs is due to the continuous CSP reset through the feedback resistor. The voltage pulses, shown in Fig. 7, range from about 200 mV to about 350 mV. These values multiplied by the CSP sensitivity give charge values in the range of 26–45 fC. The obtained charges can be converted to the energy deposited in the SV²⁵ by multiplying by the mean energy required to create an electron–hole pair in diamond (i.e., 13.2 eV²⁶) and dividing by the electron charge, $e = 1.6 \times 10^{-19}\ \text{C}$, resulting in an energy range from 2.1 to 3.7 MeV.

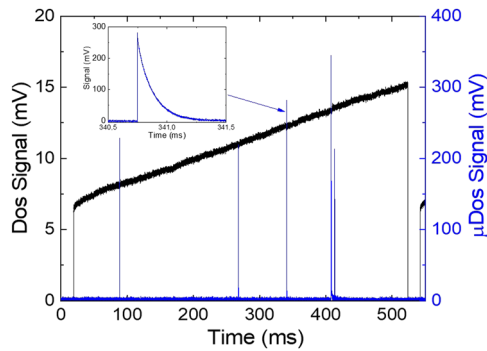


FIG. 7. Output signals from the Dos (black curve) and μ Dos (blue curve) detectors under α -particle irradiation.

Such values are consistent with the expected energy deposition distribution by the α -particles in the SV of the detector. Indeed, using Monte Carlo simulations, the mean energy deposited perpendicularly across the SV thickness ($6.4 \mu\text{m}$ in this case) is $\sim 2.1 \text{ MeV}$. The deposition of higher energies observed can be attributed to longer path lengths of α -particles crossing the SV at non-orthogonal angles (uncollimated beam).

The current generated in the SV of the Dos and the energy deposition distribution in the SV of the μ Dos were recorded simultaneously when the device was irradiated by α -particles. The pulse height analysis (PHA) spectrum of the diamond μ Dos with an SV

thickness of $2.5 \mu\text{m}$, measured under α -particle irradiation, is shown in Fig. 8(a). The PHA spectrum was acquired over a period of $\sim 12 \text{ h}$ to ensure a reasonable statistical representation. The detector response remained stable and reproducible, showing no evidence of polarization effects. The Gaussian fitting of the spectrum yielding a peak energy of $\sim 710 \text{ keV}$, which closely agrees with the Monte Carlo simulation, indicating again a 100% CCE of μ Dos. The events observed below 0.3 MeV are primarily attributed to edge effects, where incomplete charge collection occurs near the borders of the SV. In addition, the lack of collimation of the alpha particle beam significantly contributes to these low-energy events by increasing the angular spread of the incident particles and broadening their energy distribution.

The current measured by Dos detector as a function of time is shown in Fig. 8(b). The current remained stable, exhibiting a good signal-to-noise ratio within the pA range. The dark current was very low, about 0.1 pA , comparable with the leakage current in the electronic circuit. The amplitude of the current was about $1.7 \pm 0.2 \text{ pA}$, consistent with the expected values. This consistency is supported by Monte Carlo simulations, which estimate the average energy deposited, E , in the Dos device (about $1 \mu\text{m}$ thick) by a single α -particle to be around 285 keV . Given the aforementioned α -particle fluence rate, a current $i = \frac{\phi E e A_{\text{Dos}}}{13.2} \approx 1.5 \text{ pA}$ should be generated in the diamond dosimeter, aligning well with the observed measurements. These results underline the accuracy and reliability of the DIODE device under such irradiation conditions.

IV. CONCLUSION

A novel detection system based on a synthetic single crystal diamond, namely, DIODE, was developed to perform simultaneous dosimetric and microdosimetric characterizations of clinical ion beams to provide fast and reliable dosimetry in ion therapy centers, improving existing approaches. Integrated active components configured as Schottky diodes on a single diamond substrate were fabricated and tested. Characterization using the IBIC technique revealed two distinct sensitive areas confined within the metallic contact regions, underscoring the device's accurate spatial resolution and 100% charge collection efficiency. The electronic circuits for both detectors work as expected; even in the integrated housing, the noise interferences are negligible. Dos electronic components exhibit a leakage current of about 0.1 pA and a wide current dynamic range, while the μ Dos ones achieve an energy resolution of $4.3 \text{ keV}_{\text{FWHM}}$ in diamonds and a high sensitivity of about 7.7 V/pC . The dedicated front-end electronics and waterproof housing ensured minimal noise and portability. Laboratory tests using alpha particles emitted from an ^{241}Am source in the air produced encouraging results with a particularly good signal-to noise ratio. Tests of continuous acquisition for several hours demonstrated stable and reproducible responses. Future tests on clinical beams using protons and carbon ions are in progress to further validate the performance of the DIODE system.

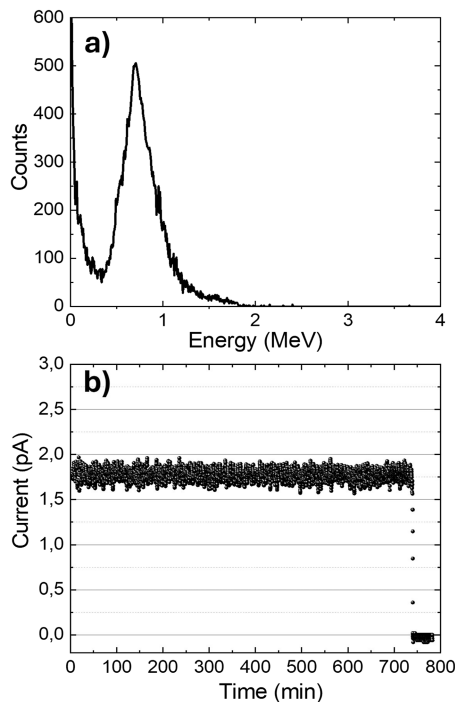


FIG. 8. (a) PHA spectrum acquired by μ Dos and (b) current from Dos as a function of time under α -particles irradiation.

ACKNOWLEDGMENTS

This work was supported by the National Institute of Nuclear Physics, INFN-DIODE project founded by CSNV.

AUTHOR DECLARATIONS

Conflict of Interest

The authors have no conflicts to disclose.

Author Contributions

C. Verona: Conceptualization (lead); Data curation (lead); Investigation (equal); Resources (lead); Writing – original draft (lead). **A. Fabbri:** Conceptualization (equal); Investigation (equal); Methodology (equal); Software (lead); Writing – review & editing (equal). **A. Fazzi:** Conceptualization (equal); Investigation (equal); Methodology (equal); Writing – review & editing (equal). **L. Bianchi:** Formal analysis (equal); Writing – review & editing (equal). **V. Conte:** Writing – review & editing (equal). **G. Petringa:** Writing – review & editing (equal). **A. Raso:** Writing – review & editing (equal). **G. Verona Rinati:** Conceptualization (equal); Writing – review & editing (equal).

DATA AVAILABILITY

The data that support the findings of this study are available from the corresponding author upon reasonable request.

REFERENCES

- ¹See <https://www.ptcog.site/index.php/facilities-in-operationpublic> for more information about particle therapy facilities.
- ²M. Durante and J. S. Loeffler, “Charged particles in radiation oncology,” *Nat. Rev. Clin. Oncol.* **7**, 37–43 (2010).
- ³D. Schardt, T. Elsässer, and D. Schulz-Ertner, “Heavy-ion tumor therapy: Physical and radiobiological benefits,” *Rev. Mod. Phys.* **82**, 383–425 (2010).
- ⁴Y. Matsumoto, N. Fukumitsu, H. Ishikawa *et al.*, “A critical review of radiation therapy: From particle beam therapy (proton, carbon, and BNCT) to beyond,” *J. Pers. Med.* **11**(8), 825 (2021).
- ⁵H. Fuji, U. Schneider, Y. Ishida, M. Konno, H. Yamashita, Y. Kase, S. Murayama, T. Onoe, H. Ogawa, H. Harada, H. Asakura, and T. Nishimura, “Assessment of organ dose reduction and secondary cancer risk associated with the use of proton beam therapy and intensity modulated radiation therapy in treatment of neuroblastomas,” *Radiat. Oncol.* **8**, 255 (2013).
- ⁶G. Giovannini, T. Böhlen, G. Cabal, J. Bauer, T. Tessonier, K. Frey, J. Debus, A. Mairani, and K. Parodi, “Variable rbe in proton therapy: Comparison of different model predictions and their influence on clinical-like scenarios,” *Radiat. Oncol.* **16**(1), 59 (2021).
- ⁷A. Verkhovtsev, E. Surdutovich, and A. V. Solovyov, “Phenomenon-based evaluation of relative biological effectiveness of ion beams by means of the multiscale approach,” *Cancer Nanotechnol.* **8**(1), 12 (2017).
- ⁸A. B. Rosenfeld, G. I. Kaplan, M. C. Carolan, B. J. Allen, R. Maughan, M. Yudelev, C. Kota, and J. Coderre, “Simultaneous macro and micro dosimetry with MOSFETs,” *IEEE Trans. Nucl. Sci.* **43**(6), 2693–2700 (1996).
- ⁹G. Magrin, H. Palmans, M. Stock, and D. Georg, “State-of-the-art and potential of experimental microdosimetry in ion-beam therapy,” *Radiother. Oncol.* **182**, 109586 (2023).
- ¹⁰P. Colautti, G. Magrin, H. Palmans, M. A. Cortés-Giraldo, and V. Conte, “Characterizing radiation effectiveness in ion-beam therapy Part II: Microdosimetric detectors,” *Front. Phys.* **8**, 550458 (2020).
- ¹¹L. T. Tran, D. Bolst, B. James, V. Pan, J. Vohradsky, S. Peracchi, L. Chartier, E. Debrot, S. Guatelli, M. Petasecca, M. Lerch, D. Prokopovich, Ž. Pastuović, M. Povoli, A. Kok, T. Inaniwa, S. H. Lee, N. Matsufuji, and A. B. Rosenfeld, “Silicon 3D microdosimeters for advanced quality assurance in particle therapy,” *Appl. Sci.* **12**, 328 (2021).
- ¹²C. Guardiola, C. Fleta, D. Quirion, G. Pellegrini, and F. Gómez, “Silicon 3D microdetectors for microdosimetry in hadron therapy,” *Micromachines* **11**, 1053 (2020).
- ¹³C. Verona, G. Magrin, P. Solevi, V. Grilj, M. Jakšić, R. Mayer, M. Marinelli, and G. Verona-Rinati, “Spectroscopic properties and radiation damage investigation of a diamond based Schottky diode for ion-beam therapy microdosimetry,” *J. Appl. Phys.* **118**, 184503 (2015).
- ¹⁴J. A. Davis, P. Lazarakis, J. Vohradsky, M. L. Lerch, M. Petasecca, S. Guatelli, and A. B. Rosenfeld, “Tissue equivalence of diamond for heavy charged particles,” *Radiat. Meas.* **122**, 1–9 (2019).
- ¹⁵M. Marinelli, F. Pompili, G. Prestopino, C. Verona, G. Verona-Rinati, G. Cirrone, G. Cuttone, R. La Rosa, L. Raffaele, F. Romano, and C. Tuve, “Dosimetric characterization of a synthetic single crystal diamond detector in a clinical 62 MeV ocular therapy proton beam,” *Nucl. Instrum. Methods Phys. Res., Sect. A* **767**, 310–317 (2014).
- ¹⁶A. K. Mandapaka, A. Ghebremedhin, B. Patyal, M. Marinelli, G. Prestopino, C. Verona, and G. Verona-Rinati, “Evaluation of the dosimetric properties of a synthetic single crystal diamond detector in high energy clinical proton beams,” *Med. Phys.* **40**, 121702 (2013).
- ¹⁷C. Verona, G. V. Rinati, G. Schettino, and G. Parisi, “Development and fabrication of microdosimeter arrays based on single-crystal diamond Schottky diodes,” *Physica Status Solidi A* **221**, 2300987 (2024).
- ¹⁸J. A. Davis, M. Petasecca, S. Guatelli, M. L. F. Lerch, and A. B. Rosenfeld, “Evolution of diamond based microdosimetry,” *J. Phys.: Conf. Ser.* **1154**, 012007 (2019).
- ¹⁹I. A. Zahradnik, M. T. Pomorski, L. D. Marzi, D. Tromson, P. Barberet, N. Skukan, P. Bergonzo, G. Devès, J. Herault, W. Kada, T. Pourcher, and S. Saada, “scCVD diamond membrane based microdosimeter for hadron therapy,” *Physica Status Solidi A* **21**, 18003832 (2018).
- ²⁰O. Loto, I. Zahradnik, A. Leite, L. De Marzi, D. Tromson, and M. Pomorski, “Simultaneous measurements of dose and microdosimetric spectra in a clinical proton beam using a scCVD diamond membrane microdosimeter,” *Sensors* **21**, 1314 (2021).
- ²¹C. Verona, S. Barna, D. Georg, Y. Hamad, G. Magrin, M. Marinelli, C. Meouchi, and G. Verona Rinati, “Diamond based integrated detection system for dosimetric and microdosimetric characterization of radiotherapy ion beams,” *Med. Phys.* **51**, 533–544 (2024).
- ²²I. Ciancaglioni, C. Di Venanzio, M. Marinelli, E. Milani, G. Prestopino, C. Verona, G. Verona-Rinati, M. Angelone, M. Pillon, and N. Tartoni, “Influence of the metallic contact in extreme-ultraviolet and soft x-ray diamond based Schottky photodiodes,” *J. Appl. Phys.* **110**, 054513 (2011).
- ²³J. Allison *et al.*, “Recent developments in geant4,” *Nucl. Instrum. Methods Phys. Res., Sect. A* **835**, 186–225 (2016).
- ²⁴E. Vittone, “Semiconductor characterization by scanning ion beam induced charge (IBIC),” *Microscopy, Int. Scholarly Res. Not.* **2013**, 637608 (2013).
- ²⁵C. Leroy and P. Rancoita, *Principles of Radiation Interaction in Matter and Detection* (World Scientific Publishing, 2016).
- ²⁶G. J. Schmid, J. A. Koch, R. A. Lerche, and M. J. Moran, “A neutron sensor based on single crystal CVD diamond,” *Nucl. Instrum. Methods Phys. Res., Sect. A* **527**, 554 (2004).